Boundary Layer Characteristics of the Miley Airfoil at Low Reynolds Numbers

Lawrence J. Pohlen* and Thomas J. Mueller†
University of Notre Dame, Notre Dame, Indiana

An experimental study of the effect of boundary-layer transition on the performance of the Miley airfoil at Reynolds numbers below 6×10^5 was conducted. Lift and drag measurements were taken using a two-component strain gage force balance over a range of Reynolds numbers from 7×10^4 to 3×10^5. Static pressure distributions on the surface of the airfoil were measured for Reynolds numbers up to 6×10^5. Smoke flow visualization was used at Reynolds numbers between 7×10^4 and 5×10^5 in order to obtain a qualitative picture of boundary-layer transition and flow separation. Initial studies showed a large region of hysteresis in both lift and drag performance between Reynolds numbers of 7×10^4 and 1.5×10^5. The hysteresis loop varied in size but typically occurred between 10- and 18-deg angle of attack and resulted in up to a 75% difference in lift coefficient and up to a 60% difference in drag coefficient. Stability of the hysteresis loop was found to be dependent on several factors, most important of which were freestream turbulence, acoustic excitation, and boundary-layer trips. The test section environment was documented to explain changes in boundary-layer performance under normal operating conditions. Finally, quantitative analysis of the boundary-layer performance was conducted with a hot-wire anemometer at 0-, 7-, and 13-deg angle of attack for a Reynolds number of 1.5×10^5. Comparison of the data obtained during the different experimental phases provides a consistent picture of the boundary-layer performance and subsequent hysteresis loop. Changes in the testing environment were found to be the critical factors in variations of the experimental results. Documentation of the test environment is a prerequisite to the analysis of any test results at low Reynolds numbers.

Nomenclature

c = airfoil chord, cm
C_d = section profile drag coefficient
C_f = force coefficient
C_ℓ = section lift coefficient
C_m = moment coefficient
C_p = pressure coefficient $= (P_i - P_\infty)/Q_\infty$
H_{12} = shape factor equal to the boundary-layer displacement thickness divided by the momentum thickness
H_{32} = shape factor equal to the boundary-layer energy thickness divided by the momentum thickness
P = static pressure, mm Hg or mm H_2O
Q = dynamic pressure, $\frac{1}{2}\rho U^2$, N/m^2
R_c = Reynolds number based on airfoil chord
S = airfoil planform area, cm^2
U = velocity in streamwise direction
x = distance along airfoil from leading edge, cm
α = angle of attack, deg
δ_1 = boundary-layer displacement thickness, cm
δ_2 = boundary-layer momentum thickness, cm
δ_3 = boundary-layer energy thickness, cm
μ = absolute fluid viscosity, kg/m/s
ρ = density of fluid, kg/m^3

Subscripts

$c/4$ = quarter-chord values
d = drag related values
i = referring to pressure tap numbers i
ℓ = lift related values
max = maximum value for variable
min = minimum value for variable
∞ = freestream value

Received Aug. 25, 1983; revision received April 11, 1984.

*Graduate Research Assistant, Department of Aerospace and Mechanical Engineering; currently stationed at USAF Space Division, Los Angeles, Calif. Member AIAA.

†Professor, Department of Aerospace and Mechanical Engineering. Associate Fellow AIAA.

Introduction

RECENTLY, attention has turned toward low-speed airfoil design in an effort to obtain better performance for both military and civilian systems. These applications include jet engine compressor and turbine blades, remotely piloted vehicles (RPV's) at high altitudes, sailplanes, ultralight man-carrying/manpowered aircraft, and mini-RPV's at low altitudes. These systems require efficient airfoil sections in the chord Reynolds number range from about 100,000 to about 1,000,000.

Many of the problems which occur at low Reynolds numbers have been known since the early 1900's; however, the first systematic study of these was accomplished by Schmitz[1] in the early 1940's. This work, which originally was directed toward model airplane applications, has served as an important basis for many subsequent studies. Many significant aerodynamic problems occur below chord Reynolds numbers of about 500,000.[2] Although some progress has been made, there are problems requiring more study if further improvements are to be realized. These problems are related to the management of the airfoil boundary layer and the difficulties related to making accurate wind tunnel[3] and free-flight measurements.[4] In relation to the airfoil boundary layer, important areas of concern are the separated regions which occur near the leading and/or trailing edges and transition from laminar to turbulent flow.[2] It is well known that separation and transition are highly sensitive to Reynolds number, pressure gradient and the disturbance environment.[5] Transition and separation play a critical role in determining the development of the boundary layer which, in turn, affects the overall performance of the airfoil.[2]

Many of the problems plaguing low Reynolds number research involve difficulties associated with making accurate

wind tunnel models and obtaining reliable data Because the airfoil boundary layers are sensitive to small disturbances, accurate wind tunnel models are very important in the evaluation of a given design Furthermore, because the forces, pressure differences, and velocities are small, a great deal of care must be exercised to obtain accurate and meaningful data

The airfoil designed by Miley[4] using the philosophy suggested by Wortmann and the mathematical techniques developed by Eppler was chosen for these experiments The design velocity distribution and the resulting airfoil section, designated the M06 13 128, are shown in Fig 1 This airfoil was designed for $C_\ell = 1\ 31$, $C_d = 0\ 012$ at $\alpha = 11$ deg, and a chord Reynolds number of 600,000 Some flight data was obtained by Miley[4] using a two dimensional airfoil with end plates mounted on a glider Although this airfoil section also was used in the Mini Sniffer RPV,[6] there appears to be no detailed data available on the boundary layer characteristics

The primary objective of the present research is to obtain a better understanding of the occurrence and behavior of transition and/or separation, as well as their effect on the overall performance of airfoils, using the unique low speed smoke tunnels at Notre Dame To meet this goal, data are required on the detailed characteristics of the boundary layer The sensitivity of the separation and transition to pressure gradient, i e , airfoil shape and angle of attack, and free stream disturbance, are important in understanding this complex flow phenomenon and improving analytical tech niques of predicting it

Experimental Apparatus

An indraft wind tunnel with external strain gage balance was used to obtain the force measurements The wind tunnel test section is 610 mm square and 1828 mm long A complete description of the wind tunnel facility is given in Ref 3 The flow visualization, pressure, and hot wire experiments were made in an identical test section, with the model and side plates rotated 90 deg from the force balance configuration, i e , airfoil horizontal The smoke wire technique was used to visualize the flow around the airfoil at low Reynolds numbers Turbulence screens are introduced upstream of the model to increase turbulence intensities, and flow restrictors were placed downstream of the model to reduce test section velocities

Experiments were performed using two Miley airfoil models cast from the same mold These smooth models each had a chord of 250 mm and a span of 421 mm One model was used as a full span force model and for flow visualization and hot wire experiments The other model was cast with 90 static pressure taps for pressure measurements.

Description of Disturbance Environment

The disturbance environment was documented by measuring the acoustic and turbulence levels in the test section for a range of velocities [5] Turbulence intensities in the standard wind tunnel configuration increased from 0 07% at 9 m/s to 0 15% at 31 m/s Higher turbulence intensities were produced in the test section when the motor was operating at 460 rpm due to pulsation of the fan Introduction of a flow restrictor increased the freestream turbulence for a given fan rpm The pulsating disturbance at 460 rpm was magnified with flow restrictors in place No attempt was made to determine un certainties in the absolute magnitude of the turbulence in tensities It was more desirable for this analysis to accurately document the relative change in turbulence intensities between different test conditions in order to understand changes in airfoil performance

Documentation of the acoustic environment showed a primary dependence on the fan rpm Sound pressure levels increased directly with increases in fan speed Introduction of flow restrictors caused the sound pressure level at a given velocity to increase because of the requirements for larger fan rpms to produce the same velocity Freestream turbulence and sound pressure levels had distinct characteristic frequencies associated with the fan blade passage frequency Introduction of flow restrictors amplified these characteristic frequencies Turbulence screens produced larger freestream turbulence intensities with no characteristic frequencies in the 0 500 Hz range

Airfoil Performance

Lift and Drag Force Data

Lift and drag performance between Reynolds numbers of 70,000 and 300,000 presents some very interesting and im portant trends Airfoil lift and drag hysteresis was found to occur in the Reynolds number range between 70,000 and 150,000 On the graphs presented here arrows indicating the direction of the hysteresis have been drawn to assist in the discussion The hysteresis found on the Miley airfoil is very unusual in that its performance is worse as angle of attack is increased than it is as the angle of attack is decreased from a value beyond stall The most common type of hysteresis occurs when flow reattachment occurs at a lower angle than the separation of "stall" angle No attempt was made to

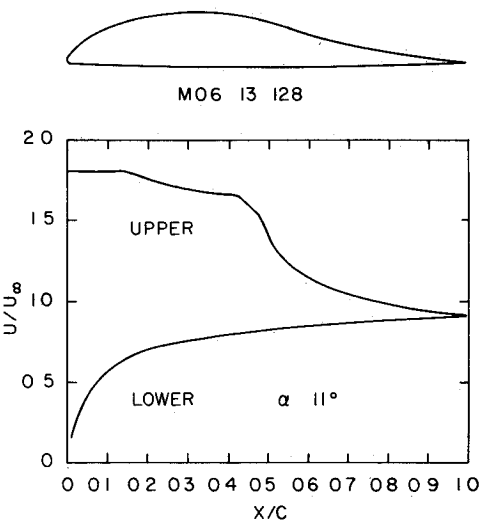

Fig 1 The design velocity distribution and the resulting airfoil (designated the M06 13 128)

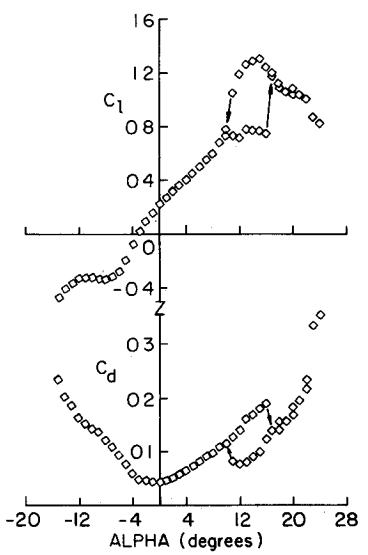

Fig 2 Section lift and drag coefficients vs angle of attack; corrected for blockage $R_c = 100\ 000$; one flow restrictor

investigate hysteresis at negative angles of attack Lift and drag coefficients are plotted in Figs 2 5 for Reynolds numbers of 100,000 and 300 000 All coefficients are corrected for tunnel blockage, etc [7]

The hysteresis phenomenon is best described at $R_c = 100\,000$ Figure 2 illustrates the airfoil performance at $R_c = 100{,}000$ The lift curve slope at lower angles of attack, as angle of attack increases from -3 to 10 deg, is 0 054/deg However the lift levels off at $\alpha = 10$ deg and remains relatively constant until it increases drastically with the formation of a separation bubble at 17 deg A gradual decrease in lift occurs thereafter, with leading edge stall occurring at $\alpha = 23$ deg In contrast the lift is maintained as angle of attack is decreased from $\alpha = 23$ deg A maximum lift coefficient of 1 31 occurs at $\alpha = 15$ deg As the angle of attack decreases from 15 deg the lift decreases gradually with a large drop occurring at 10 deg The location of the hysteresis loop shifts to lower angles of attack as the Reynolds number in creases The hysteresis loops in the drag curves coincide with the lift as is expected The minimum drag coefficient occurs at -1 deg

Figures 3 and 4 show two cases of lift and drag performance at $R_c = 150\,000$ The first occurs with a flow restrictor in place and the second with no flow restrictor in use There is a marked difference in performance There is no hysteresis when the flow restrictor is used With the flow restrictor in place, the lift curve slope changes at approximately 7 deg improving to 0.085/deg Maximum lift occurs at 14 deg and a gradual decrease in lift occurs thereafter. In contrast the lift curve slope levels off at $\alpha = 10$ deg and remains constant at approximately 0 78 through $\alpha = 17$ deg for the no flow restrictor case. Drag performance with the flow restrictor in place is much improved A drag "bump" occurs between $\alpha = 2$ deg and $\alpha = 10$ deg but no hysteresis is observed $C_{d\min}$ is slightly lower for the no flow restrictor case, however, overall drag performance is improved with the flow restrictor in place. It should be noted that the hysteresis loop at $R_c = 150{,}000$ was very unstable $R_c = 150{,}000$ appears to be an upper limit to the formation of the loop Fluctuating tunnel velocities or abrupt movement of the airfoil through changes in angle of attack wiped out the hysteresis

Figure 5 shows the performance of the Miley airfoil at $R_c = 300{,}000$ The lift curve slope continues to increase with increasing Reynolds number and the discontinuity that occurs at $\alpha = 7$ deg begins to disappear The corresponding bump in the drag curve also disappears At $R_c = 300{,}000$ the lift curve slope is 0 086/deg and a $C_{\ell_{max}}$ of 1 4 occurs at 14 deg followed by a gentle decrease in lift A drag bucket has formed between $\alpha = -1$ and 12 deg with drag coefficients between 0 025 and 0 04

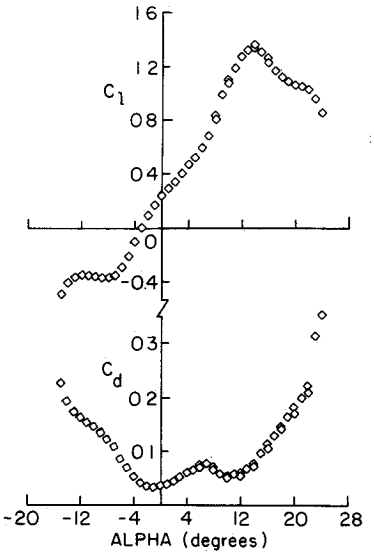

Fig 3 Section lift and drag coefficients vs angle of attack; corrected for blockage $R_c = 150{,}000$; one flow restrictor

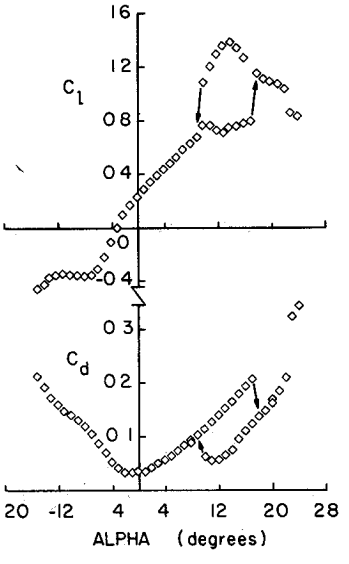

Fig 4 Section lift and drag coefficients vs angle of attack; corrected for blockage $R_c = 150{,}000$; no flow restrictor

Pressure Measurements

Analysis of the pressure data was performed in two steps Plots of the pressure distributions were analyzed for separation and bubble formation in the airfoil boundary layer, and then the pressure distributions were integrated using a trapezoidal analog to give an indication of lift and drag performance Moment coefficients were also calculated to provide information on pitching performance All pressure coefficients presented here are corrected for blockages, etc Lift coefficients calculated from the pressure measurements were regularly within 2 or 3% of those measured by the force balance Drag coefficients showed an identical behavior with those measured by the force balance, including the hysteresis and drag bump phenomena However, comparison of drag coefficient magnitudes varied up to 15% Integration of drag requires the calculation of small components of pressure over extremely small areas which produces a wide margin of error

Analysis of the pressure distributions themselves, provides a better understanding of boundary layer behavior Regions in the pressure distribution (after an adverse pressure gradient) where the pressure coefficients remain constant, represent separated regions Leading-edge separation bubbles are characterized by a small plateau followed by a steep gradient and a change in the pressure slope where reat tachment takes place. Where applicable, separation, transition, and reattachment are indicated for the upper surface by s t or r, respectively

Pressure distributions for $R_c = 100{,}000$ are presented in Fig 6 At $\alpha = -9$ deg the bottom surface is effectively stalled, while a long bubble is formed on the top surface The laminar flow separates at $x/c = 0\ 48$, transitions to turbulent flow at approximately $x/c = 0\ 70$, and reattaches at $x/c = 0\ 8$ after which it begins to accelerate toward the trailing edge At $\alpha = -3$ deg, the zero lift angle, the long bubble is still present on the upper surface, but reattachment has been delayed to $x/c = 0\ 92$ The long bubble at $\alpha = 0$ deg reattaches near the trailing edge, while reattachment on the airfoil never occurs at $\alpha = 7$ deg Leading edge acceleration increases through $\alpha = 9$, 13, and 15 deg as separation of the laminar boundary layer moves toward the leading edge, Figs 6a g At $\alpha = 19$ deg a short leading edge separation bubble has formed The for mation of the bubble improves the lift performance drastically At $\alpha = 23$ deg the flow separates at the leading

edge As the angle of attack is decreased from stall, the bubble reforms As α is decreased further the separation bubble begins to shrink At $\alpha = 17$ deg (decreasing) the bubble length has shrunk to 2 3% of the chord At $\alpha = 15$ deg there is no indication of bubble formation The boundary layer remains attached and a large suction peak is maintained when the bubble disappears The pressure distribution at $\alpha = 15$ deg (decreasing) was not obtained unless the bubble was first formed at higher angles of attack and the angle of attack then decreased. The pressure distribution at $\alpha = 13$ deg is very similar to the theoretical distribution designed by Miley In this case transition of the boundary layer would be expected to occur at $x/c = 0$ 35 Actual transition may occur nearer the leading edge for this case The high performance boundary layer at $\alpha = 13$ deg was unstable and often collapsed to the lower performance case causing a change in the pressure distribution

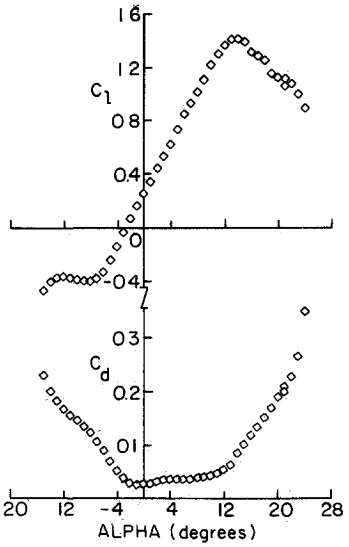

Fig 5 Section lift and drag coefficients vs angle of attack; corrected for blockage $R_c = 300{,}000$; no flow restrictor

Improved performance is documented by the pressure distributions at $R_c = 300{,}000$ in Fig 7a j A long bubble forms at $\alpha = -9$ deg as before, but the transition point is much closer to separation than it was at lower Reynolds numbers The bubble remains stable at $\alpha = -3$ and 0 deg with transition occurring just after separation A large improvement in the performance of the airfoil is noted at $\alpha = 7$ deg The boundary layer remains attached over the entire length of the airfoil as transition occurs in the attached boundary layer due to the instability gradient between $x/c = 0$ 15 and 0 50 A constant pressure peak forms at $\alpha = 11$ deg and the pressure distribution shown in Fig 7f is the theoretical distribution predicted by Miley with a slightly lower initial suction peak As the angle is increased above 11 deg (Figs 7g j), the suction peak increases further and the adverse pressure gradient steepens A trailing edge stall begins at $\alpha = 15$ deg and is completed at $\alpha = 23$ deg, producing a gradual stall in the lift curve

Summary of Performance

Figures 8 10 present a summary of airfoil performance obtained from the force balance and pressure distribution measurements Maximum lift and minimum drag coefficients are presented with the calculated uncertainty Maximum lift coefficients show a drastic improvement from a Reynolds

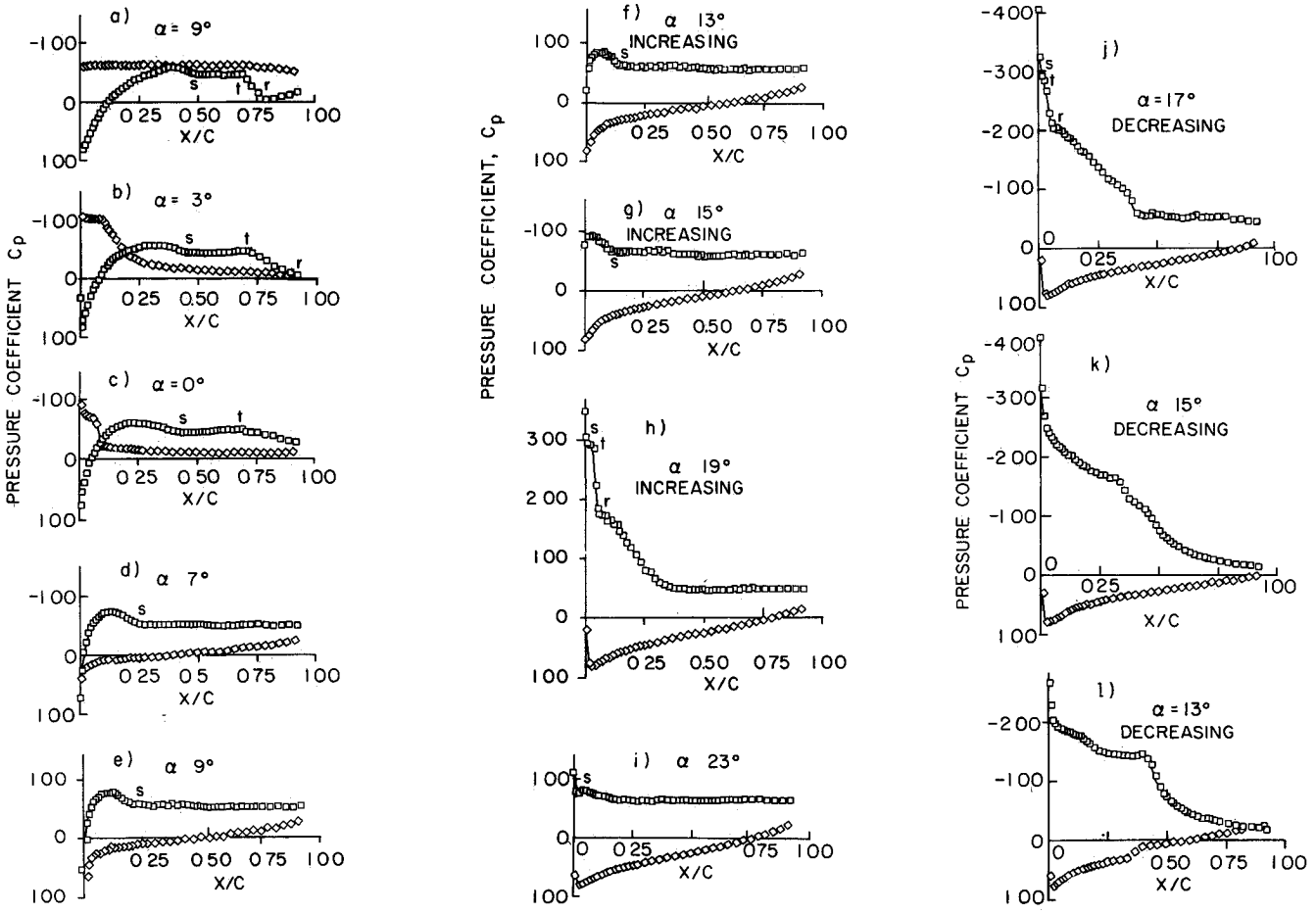

Fig 6 Static pressure coefficients vs nondimensional position along the airfoil chord at $R_c = 100{,}000$ with one flow restrictor

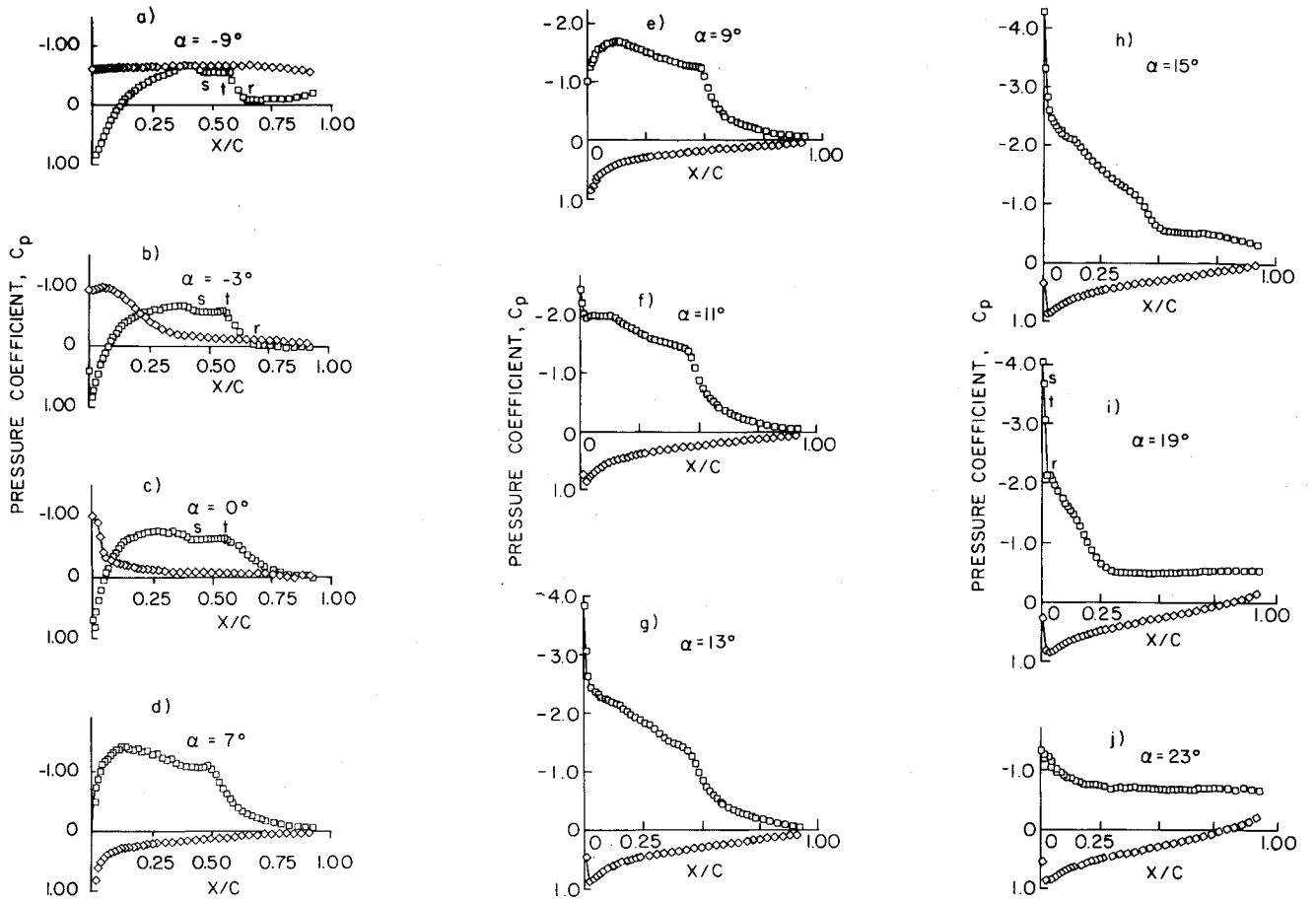

Fig. 7 Static pressure coefficients vs nondimensional position along the airfoil chord at $R_c = 300{,}000$ with no flow restrictor.

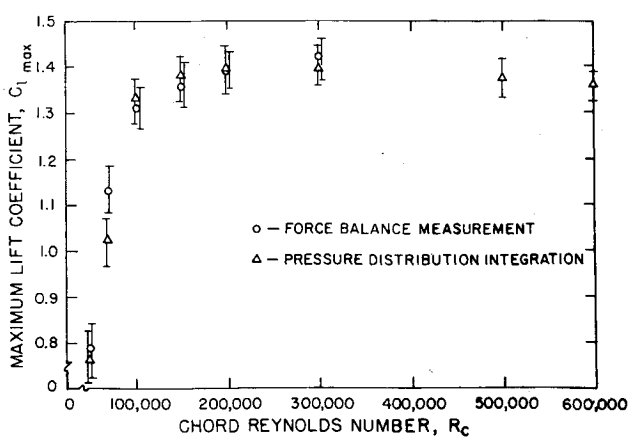

Fig. 8 Maximum section lift coefficient vs chord Reynolds number with uncertainty estimates.

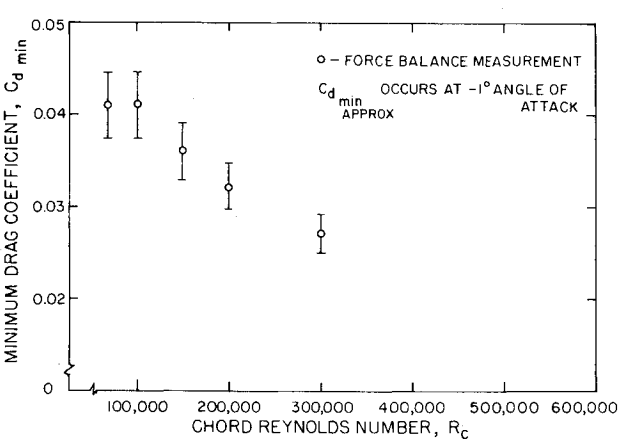

Fig. 9 Minimum section profile drag coefficient vs chord Reynolds number with uncertainty estimates.

number of 55,000 to 150,000. It should be noted that this can be deceptive since the maximum lift coefficients shown for $R_c = 70{,}000$ and 100,000 are only obtainable as the angle of attack is *decreased* from about 20 deg. Above $R_c = 150{,}000$ maximum lift coefficients remain relatively constant. Lift coefficients calculated from the pressure distribution show excellent agreement with the force data.

Minimum drag coefficients typically occur at $\alpha = -1$ deg, and decrease as Reynolds number increases. Minimum drag coefficients are independent of the hysteresis phenomenon. While the maximum lift coefficient remains constant above $R_c = 150{,}000$, the minimum drag coefficient continues to decrease through $R_c = 600{,}000$. Maximum L/D increases from around 5 at $R_c = 55{,}000$ to 29 at $r_c = 300{,}000$. Large nose-down moments ($C_{mc/4}$ positive for nose-up moments) are created at low angles of attack when the flow is separated over the aft portion of the airfoil ($R_c = 100{,}000$ and 150,000). A sharp decrease in the moment coefficient occurs when the flow reattaches. The moment coefficient is much smaller at Reynolds numbers of 300,000 and 600,000 as was expected from the design criteria.

Boundary-Layer Survey

A hot-wire anemometer was used to survey the boundary layer for four different test cases. Results obtained include velocity and turbulence intensity profiles, calculated boundary-layer parameters, and frequency spectra of boundary-layer turbulence.[8] Boundary-layer profiles were taken at 30 hot-wire stations located on the upper surface of the airfoil. At each point in the boundary layer 150 samples of velocity

and turbulence intensity were taken over a 12-s period and averaged. There were 51 points in each profile Profiles varied from 5 to 25 mm in height The critical problem in analyzing profile data was the determination of the location of the hot wire probe at the initiation of the profile measurement Special care was taken to position the probe at the same height above the surface at the initiation of each profile After the data were taken different initial probe heights were used to plot the profiles and calculate boundary layer parameters After studying the results, an initial probe height of 0 08 mm was chosen for all of the profiles This data, presented in Ref 8, was used together with the pressure and force data to clarify the boundary layer behavior and to provide the in tegral parameters for use in developing design methods

Frequency Spectra

Frequency spectra of the turbulence in the boundary layer were taken to determine the influence of disturbances in the test environment on the boundary layer Frequency spectra are presented for a 0 500 Hz range since it was found that the primary disturbances in the tunnel were in this range Spectra presented here are normalized to the maximum value in each sample

Figure 11 presents a spectra taken at $R_c = 150{,}000$ and $\alpha = 13$ deg The first spectra was taken 5 cm ahead of the leading edge (Fig 11a) and the fan blade passage of 42 Hz is clearly visible. At the leading edge (Fig 11b) this acoustic frequency has been magnified by two orders of magnitude over the other frequencies. Higher harmonics at 120 and 240 Hz are also clearly visible At $x/c = 1\ 412\%$ (Fig 11c), the width of each frequency peak has increased and the higher harmonics have increased in magnitude The amplification of the primary frequencies (40, 120, 240 Hz) has died out some what at $x/c = 11.278\%$ (Fig 11d) except for the spike at 240 Hz $x/c = 31\ 557\%$ is located near transition (Fig 11e). The fan blade frequencies have disappeared almost completely and except for a very low frequency the turbulence is broadband $x/c = 53.259\%$ is located in the turbulent boundary layer and the turbulence in the 0-500 Hz range is broadband (Fig. 11f)

Results from these experiments suggest that the acoustic and turbulence disturbances in the freestream are amplified in the laminar boundary layer causing transition earlier than expected [4] This could explain the improved performance of the Miley in the wind tunnel between $R_c = 150{,}000$ and 300,000

Concluding Remarks

Performance of the Miley airfoil at low Reynolds number was very complex, but showed consistent trends. As Reynolds numbers decreased from 200,000 to 55,000, performance of the airfoil decreased drastically in a process which produced an interesting hysteresis in the lift and drag curves The range of Reynolds numbers over which this decrease in performance occurs is dependent on the freestream disturbances and airfoil surface conditions (roughness or trips)

Airfoil performance at $R_c = 300\ 000$ approached the predicted performance for $R_c = 600{,}000$ However drag coefficients remained significantly higher than those predicted from theory [4] One reason for improved performance at Reynolds numbers below the design Reynolds number of 600,000 (down to $R_c = 300{,}000$) may be the small freestream turbulence in the tunnel (0 11%)

As the Reynolds number was decreased from $R_c = 300\ 000$ a drag rise or "bump" occurred between $\alpha = 2$ and 9 deg, corresponding to the formation of a long separation bubble at these angles of attack. The lift curve slope at these angles was also decreased significantly At $R_c = 150\ 000$ hysteresis first occurs and is a result of the long bubble (laminar separation) remaining on the airfoil above $\alpha = 9$ deg At large angles of attack $\alpha = 17$ or 18 deg a short leading edge separation bubble forms, improving the airfoil performance The short bubble bursts at $\alpha = 23$ deg resulting in a leading edge separation (stall) As the angle of attack is decreased from stall, the leading edge separation bubble reforms and remains on the airfoil below $\alpha = 18$ deg As the angle of attack decreases further, the separation bubble decreases in size and is no longer visible at $\alpha = 13$ deg However, the boundary layer remains attached At approximately $\alpha = 10$ deg the laminar boundary layer suddenly separates and the long bubble reforms over the upper surface of the airfoil As the Reynolds number decreases below 150,000 the hysteresis loop

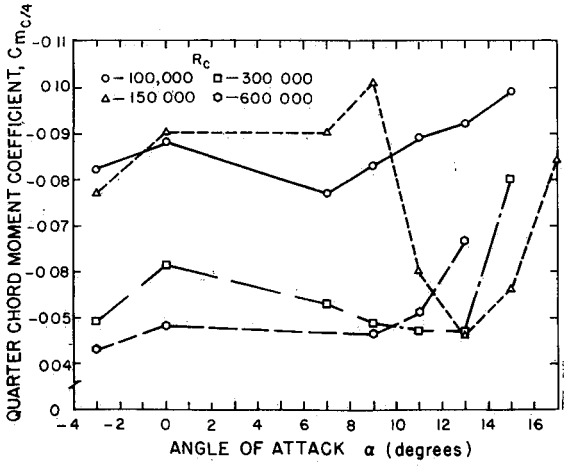

Fig 10 Quarter chord section moment coefficient vs angle of attack

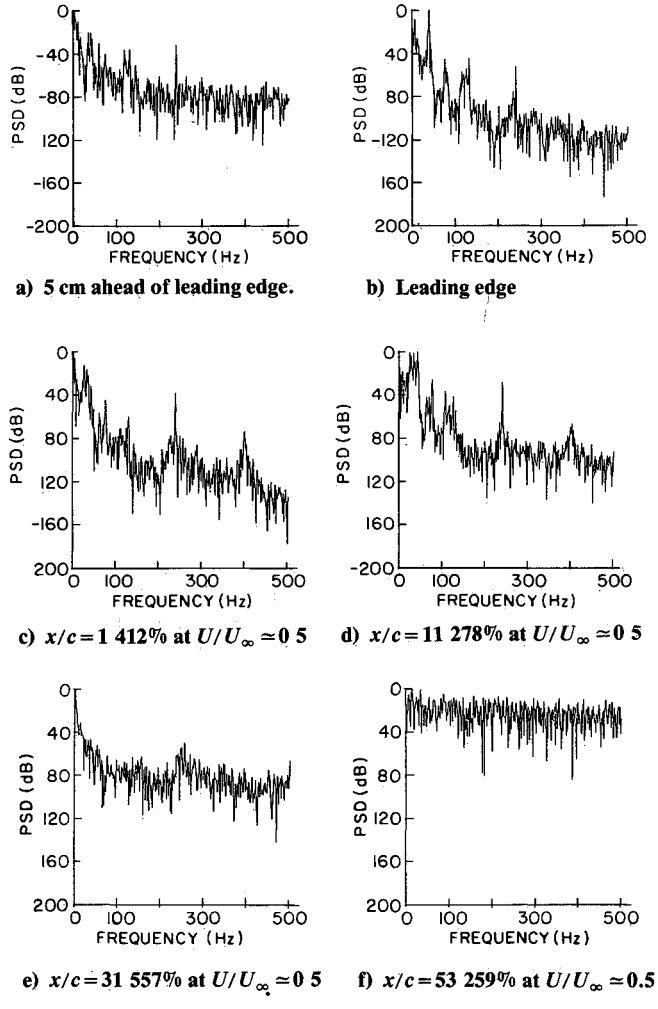

a) 5 cm ahead of leading edge. b) Leading edge

c) $x/c = 1\ 412\%$ at $U/U_\infty \simeq 0\ 5$ d) $x/c = 11\ 278\%$ at $U/U_\infty \simeq 0\ 5$

e) $x/c = 31\ 557\%$ at $U/U_\infty \simeq 0\ 5$ f) $x/c = 53\ 259\%$ at $U/U_\infty \simeq 0.5$

Fig 11 Frequency spectra for $\alpha = 13$ deg and $R_c = 150{,}000$

moves toward the higher angles of attack where a definite leading-edge separation bubble exists. Transition of the attached boundary layer does not occur as readily at the lower Reynolds numbers. The hysteresis loop begins to shrink rapidly below $R_c = 100{,}000$.

It was possible to obtain the hysteresis behavior under "normal" (no turbulence screens) operating conditions between $R_c = 70{,}000$ and 150,000. Large increases in freestream turbulence eliminated this hysteresis. Documentation of the test section environment indicated that turbulence intensities vary significantly under "normal" operating conditions depending on the number of flow restrictors used and the test Reynolds number. Changes in airfoil performance attributed to Reynolds number effects may actually be a result of changes in freestream turbulence. Hysteresis could not be generated above $R_c = 150{,}000$ in these wind tunnels. In wind tunnels with lower turbulence intensities or in turbulence free conditions (free light) the hysteresis phenomenon may occur at higher Reynolds numbers. Tests run at $R_c = 150{,}000$ with and without a flow restrictor in place showed a significant change in performance caused by changes in the test environment. Increases in turbulence intensities caused by the introduction of the flow restrictor may affect the airfoil performance (hysteresis loop) at the lower Reynolds numbers ($R_c = 70{,}000$ and 100,000).

Boundary-layer trips caused the airfoil performance to change by causing the boundary layer to transition early [8] The size of the boundary-layer trip determined the degree to which airfoil performance was altered. At $R_c = 150{,}000$, one strip of tape (2.21 mm wide and 0.127 mm thick at 1.3% chord on the upper surface) was sufficient to eliminate the hysteresis, while at $R_c = 100{,}000$ two thicknesses of this tape were required to eliminate the hysteresis completely An understanding of the effect of surface roughness provided a great deal of insight in interpreting pressure model data. The performance of the pressure model was similar to the performance of the smooth model with a single strip of tape. The surface roughness introduced by the pressure taps altered the airfoil performance significantly at low Reynolds numbers. Any surface roughness or defects in model construction could alter airfoil performance significantly.

The hot-wire anemometer survey of the boundary layer for four test cases confirmed previous results and provided a quantitative analyis of boundary-layer performance. Boundary-layer profiles at $R_c = 150{,}000$ confirmed the separation locations of $0.4c$ ($\alpha = 0$ deg) and $0.24c$ ($\alpha = 7$ deg) indicated by both the pressure measurements and flow visualization.

Calculation of boundary-layer parameters confirmed some theoretical predictions and suggested reasons for discrepancies in others. Laminar separation occurred when the shape parameter approaches $H_{32} = 1.52$ as predicted by the theory [3] The momentum thickness Reynolds number at separation was approximately $R_{\delta 2} = 220$ for both 0 and 7 deg at $R_c = 150{,}000$. Separation angles measured from flow visualization studies supported this result. Boundary-layer transition at $R_c = 150{,}000$ and $\alpha = 13$ deg took place at $R_{\delta 2} = 220$ which was lower than predictions made by Eppler or Schlichting-Ulrich-Granville.[3] Frequency spectra taken in the laminar boundary layer indicated that the characteristic frequencies present in the freestream were amplified in the laminar boundary layer. It appeared from this brief analysis that the laminar boundary layer present on the leading edge of the airfoil was receptive to the characteristic frequencies in the freestream, causing earlier transition than was predicted.[4] The receptivity of the boundary layer to turbulence and acoustic excitations in the test environment improves the airfoil performance at low Reynolds numbers. Extremely noisy test conditions may show completely different test results. Receptivity of the boundary layer may depend on the frequencies present in the freestream. No attempt was made to investigate "acoustic tripping" of the boundary layer to improve airfoil performance. However, initial results of the hot-wire survey indicate that this technique would be successful.

The results presented indicate an unusual hysteresis in the aerodynamic forces of the Miley airfoil when operated at low Reynolds numbers. This behavior is shown to be caused by the location of separation and/or transition in the airfoil boundary layer. The large amount of force, pressure distribution, and velocity data obtained delineate the problems encountered in the low Reynolds number regime and should be helpful to those involved in analytical and numerical studies of these problems.

Acknowledgments

This research was supported by the Naval Research Laboratory under Contract No. N 00014-81-K-2036 and the Department of Aerospace and Mechanical Engineering, University of Notre Dame. The authors would like to thank Dr. S. J. Miley, Dr. R. Eppler, Mr. R. J. Foch (Technical Monitor), and Drs. S. M. Batill and R. C. Nelson for their comments at various stages of this research.

References

[1]Schmitz, F W., "Aerodynamics of the Model Airplane, Part I, Airfoil Measurements," NASA-TM-X-60976, 1967.

[2]Mueller, T. J. and Batill, S. M., "Experimental Studies of the Laminar Separation Bubble on a Two-Dimensional Airfoil at Low Reynolds Numbers," AIAA Paper 80-1440, July 1980.

[3]Mueller, T J. and Jansen, B. J., Jr., "Aerodynamic Measurements at Low Reynolds Numbers," AIAA Paper 82-0598, March 1982.

[4]Miley, S. J., "An Analysis of the Design of Airfoil Sections for Low Reynolds Numbers," Ph.D. Dissertation, Mississippi State University, Miss., Jan. 1972.

[5]Mueller, T J., Pohlen, L. J., Conigliaro, P E., and Jansen, B. J., Jr., "Disturbances on Low Reynolds Number Airfoil Experiments," *Experiments in Fluids*, Vol. 1, Springer-Verlag, New York, 1983, pp. 3-14.

[6]Reed, R. D., "High Flying Mini-Sniffer RPV· Mars Bound?" *Astronautics & Aeronautics*, June 1978, pp. 26-39.

[7]Rogers, E. W E., "Blockage Effects in Closed or Open Tunnels," AGARDograph 109, 1966, pp. 279-340.

[8]Pohlen, L. J., "Experimental Studies of the Effect of Boundary Layer Transition on the Performance of the Miley (M06-13-128) Airfoil at Low Reynolds Numbers," M.S. Thesis, University of Notre Dame, Notre Dame, Ind., Jan. 1983.